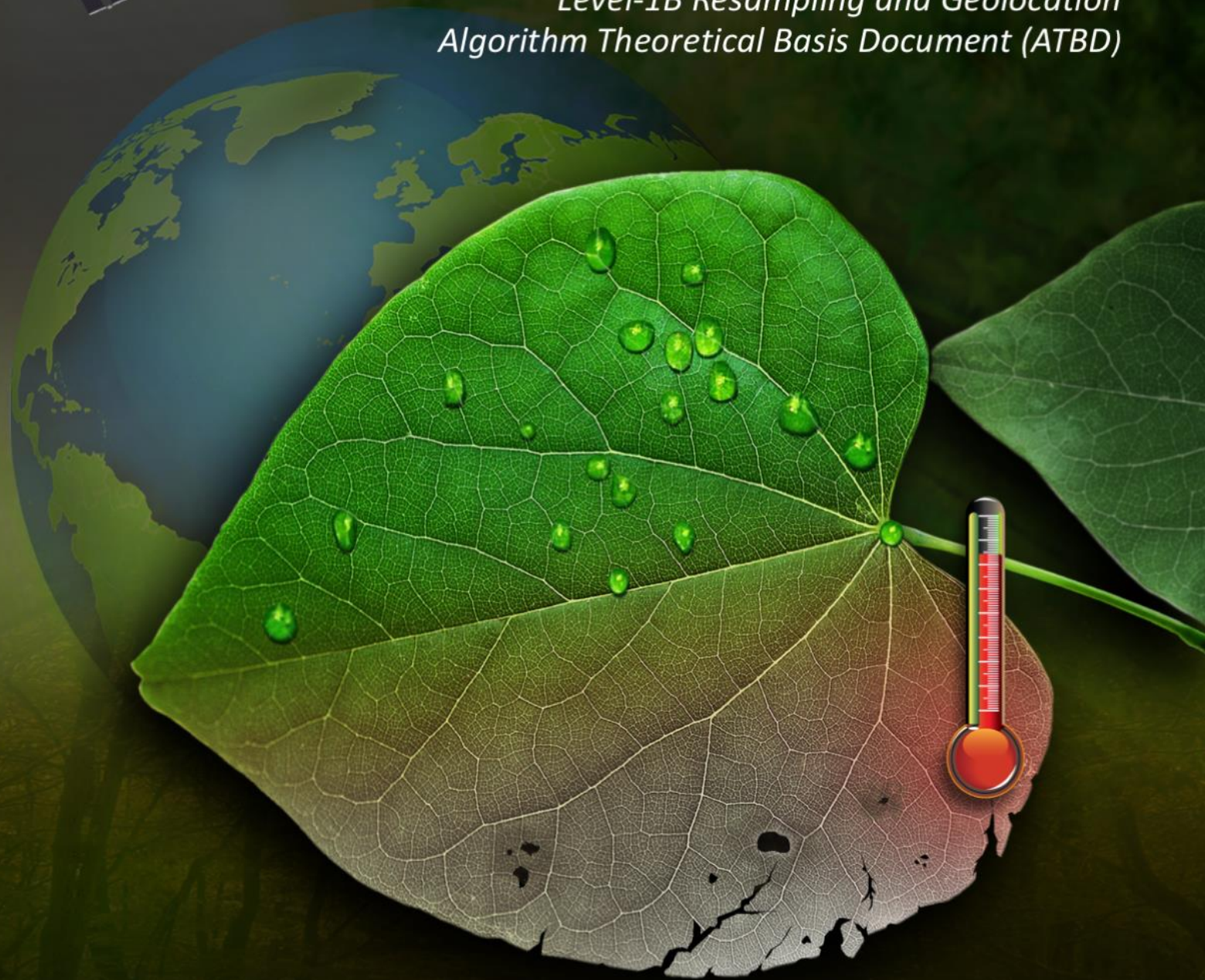




ECOSTRESS

ECOsystem Spaceborne Thermal Radiometer Experiment on Space Station

Level-1B Resampling and Geolocation Algorithm Theoretical Basis Document (ATBD)



Mike Smyth
Sebastien Leprince

Level-1 Algorithms Team

Jet Propulsion Laboratory
California Institute of Technology

Version 1.0 Rev 2
March 8, 2018

This research was carried out at the Jet Propulsion Laboratory, California Institute of Technology, under a contract with the National Aeronautics and Space Administration.

Reference herein to any specific commercial product, process, or service by trade name, trademark, manufacturer, or otherwise, does not constitute or imply its endorsement by the United States Government or the Jet Propulsion Laboratory, California Institute of Technology.

© 2018. California Institute of Technology. Government sponsorship acknowledged.

Change History Log

Revision	Effective Date	Prepared by	Description of Changes
Draft	06/30/2015	Sebastien Leprince	ECOSTRESS L1B ATBD first draft. Approved for public release, JPL Document 94641.
Version 1.0	08/20/15	Sebastien Leprince	Added 3D matrix for boresight calibration (§ 3.1)
Version 1.0 Rev 2	03/08/2018	Mike Smyth	Changed author name to Mike Smyth, since Sebastien no longer at JPL

Contacts

Readers seeking additional information about this study may contact the following:

Mike Smyth

MS 169-315

Jet Propulsion Laboratory

4800 Oak Grove Dr.

Pasadena, CA 91109

Email: *Mike.M.Smyth@jpl.nasa.gov*

Office: (818) 354-9812

Abstract

The ECOsystem Spaceborne Thermal Radiometer Experiment on Space Station (ECOSTRESS) mission was selected as a NASA Earth-Ventures Instrument (EV-I) Class-D mission on the International Space Station (ISS). Its instrument consists of a thermal infrared (TIR) multispectral scanner with five spectral bands operating between 8 and 12.5 μm . The TIR data will be acquired at a spatial resolution of 38m x 68m with a swath width of 402 km (53°) from the nominal International Space Station (ISS) altitude of 400 +/- 25 km.

This Geolocation algorithm theoretical basis document (ATBD) describes the Level 1B geolocation retrieval, and associated processing to achieve absolute georeferencing accuracy of the imagery on the order of 50 m. Largest geolocation errors are the result of inaccurate knowledge of the ISS attitude angles at the time-scale of the orbit periodicity (~ 92 min). We propose a correction of the geolocation model via image matching against a Landsat TIR imagery reference database.

Contents

Contacts	i
Abstract.....	ii
1 Introduction	5
2 ECOSTRESS Instrument Geometry and Optical Distortions	6
3 ECOSTRESS Pointing Model	9
3.1 Instrument Interior Orientation	10
3.2 From Instrument to Payload Reference Frames.....	11
3.3 From Payload to Exposed Facility Reference Frames	13
3.4 From Exposed Facility to Japanese Experiment Module Reference Frames.....	15
3.5 From Japanese Experiment Module to ISS Analysis Reference Frames.....	17
3.6 From ISS Body-Fixed to Orbital Reference Frames.....	18
3.7 From Orbital to Terrestrial Reference Frames	19
3.8 Geolocation on an Ellipsoid.....	19
3.9 Geolocation on a Topography Surface	21
4 ISS Stability Analysis	22
4.1 Expected Jitter at 1-Pixel Time-Scale.....	23
4.2 Expected Jitter at 1-Scanline Time-Scale	24
4.3 Expected Jitter at 1-Image Time-Scale	24
4.4 Expected Jitter from Repeat Orbits.....	24
4.5 Uncertainty from ISS Position Uncertainty	25
4.6 Error Budget of Geolocation.....	25
5 Geolocation Correction Based on Image Matching.....	25
5.1 Geolocation Correction Principle	26
5.2 Expected Challenges, Failures, and Worst Case Scenarios	27
6 References.....	28

Figures

Figure 1: ECOSTRESS TIR scanning scheme. Figure reproduced from [1]	6
Figure 2: Focal plane axis convention. Y is the scanning direction and X the cross-scan (ISS velocity) direction. Figure reproduced from [1].	7
Figure 3: Smearing of the pixels along the scan-direction produces elongated pixels. Figure reproduced from [1]	7
Figure 4: Left: Instrument optical distortions along the X-axis (cross-scan). Right: distortions corrected after nearest neighborhood resampling. After binning by a factor of 2, residuals are ¼ of the pixel size. Figure reproduced from [2]	8
Figure 5: Left: Instrument optical distortions along the Y (scan) direction. Right: On-board time-delay compensates for a constant offset for each spectral bands so that all bands are registered within each other within ¼ of the effective resolution. The quadratic bias that is common to all bands is accounted for in the the geolocation processing. Figure reproduced from [2]	9
Figure 6: ECOSTRESS equivalent instrument pointing model with 128 pixels in the scan direction and mirror rotation around the X-axis.	10
Figure 7: Reference system of Exposed Facility Unit (EFU) as defined in [3]	12
Figure 8: Translation of the reference systems between instrument and EFU.	12
Figure 9: Reference frame of JEM-EF, extracted from [4]	13
Figure 10: EFU10 to JEM-EF reference systems from [3]	14
Figure 11: JEM reference frame from [4]	15
Figure 12: Relative positions of JEM and EF modules from [5]	16
Figure 13: ISS Analysis Coordinate System from [4] and ECOSTRESS location	17
Figure 14: Orbital reference system definition [4]	18
Figure 15: Iterative scheme to derive geolocation using a DEM and ray intersection with ellipsoid at successive heights.	22
Figure 16: Power Spectral Density (PSD) recorded on the JEM-EF platform for all 3 axis (3 colors). The black line represents the 0.001 deg/axis expected attitude knowledge of the ISS. Reproduced from [3]	23
Figure 17: General scheme to update ECOSTRESS absolute attitude uncertainty	27

1 Introduction

The ECOsystem Spaceborne Thermal Radiometer Experiment on Space Station (ECOSTRESS) mission consists of a thermal infrared (TIR) multispectral scanner with five spectral bands operating between 8 and 12.5 μm . The TIR data will be acquired at a spatial resolution of 38m x 68m with a swath width of 402 km (53°) from the nominal International Space Station (ISS) altitude of 400 +/- 25 km.

The purpose of this document is to highlight the main physical characteristics of the ECOSTRESS instrument and of the ISS platform it is mounted on, to derive an accurate model of the instrument pointing geometry.

In the first section, we will describe the known focal-plane distortions and the associated correction using resampling. In a second section, we will derive a physical pointing model for all image pixels, along with geolocation parameters. The third section will briefly study the position and attitude characteristics of the ISS to derive absolute and relative pixel geolocation accuracy. This study is particularly important because the ECOSTRESS instrument does not carry its own inertial unit or star-tracker, and will therefore only rely on the position and attitude data broadcast by the ISS for raw geolocation determination. Suffering some inaccuracies, the knowledge of the broadcast position and attitude data will need to be augmented with post-processing to achieve the desired geolocation accuracy of the imagery. Therefore, section four will propose a geolocation correction based on image matching with a TIR ortho-image reference database. Potential limitations will be discussed.

2 ECOSTRESS Instrument Geometry and Optical Distortions

The TIR instrument operates as a push-whisk mapper 256 pixels in the cross-whisk direction for each spectral channel, which enables a wide swath and high spatial resolution. As the ISS moves forward, the scan mirror sweeps the focal plane ground projection in the cross-track direction. The different spectral bands are swept across a given point on the ground sequentially. From the 400 ± 25 -km ISS altitude, the resulting swath is 402 km wide. A wide continuous swath is produced even with an ISS yaw of up to $\pm 18.5^\circ$. A conceptual layout for the instrument is shown in Figure 1. The scan mirror rotates at a constant angular speed. It sweeps the focal plane image 53° across nadir.

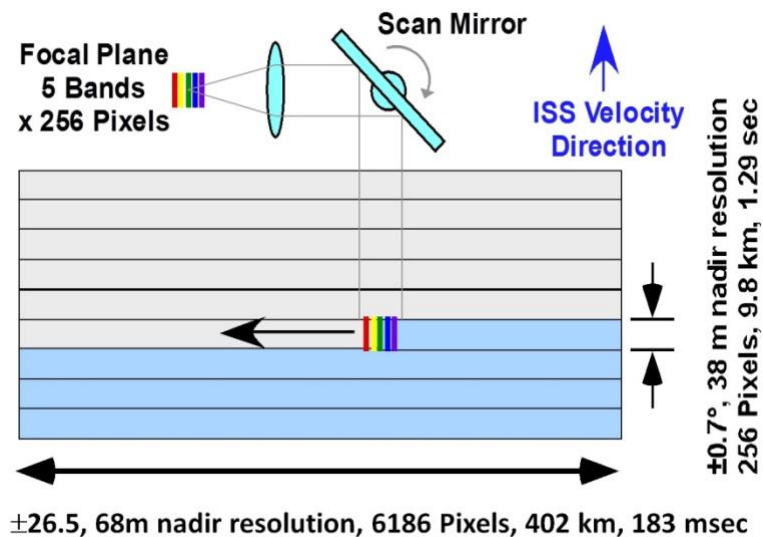


Figure 1: ECOSTRESS TIR scanning scheme. Figure reproduced from [1]

Figure 2 provides a more detailed view of the focal plane array, with corresponding axis along the scanning and cross-scanning directions. Compared to the ground ISS velocity, the high scanning velocity during the sensor dwell time of 31.6 μ s produces a smearing of the pixels

along the scanning direction, resulting in an effective nadir resolution of 68.51m along the sensor Y direction (scan direction). See Figure 3.

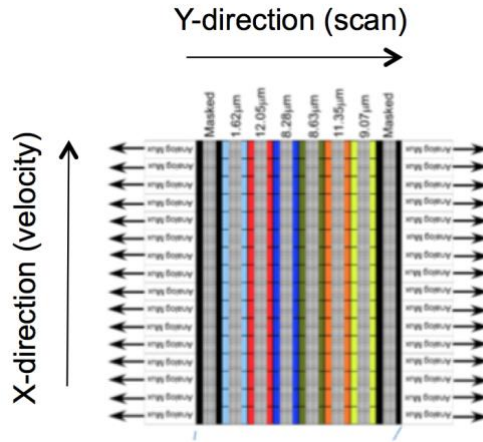


Figure 2: Focal plane axis convention. Y is the scanning direction and X the cross-scan (ISS velocity) direction. Figure reproduced from [1].

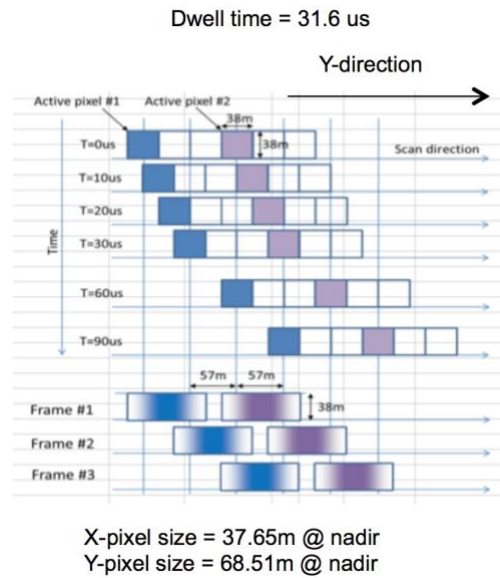


Figure 3: Smearing of the pixels along the scan-direction produces elongated pixels. Figure reproduced from [1]

Figure 4 shows the optical distortions for each pixel of each spectral band along the X direction of the sensor (cross-scan). The units of apparent deformation are in pixels, and the optics has a diverging bias along this component. A resampling procedure, applied on the ground, compensates for this bias using nearest neighborhood resampling. Using nearest neighborhood resampling, the maximum distortion that remains is equal to $\frac{1}{2}$ the size of a pixel (Figure 4, right). However, because of the smearing of the pixels in the Y (scan) direction by almost a factor of two, it is chosen to down-sample the X-component by a factor of 2 to produce imagery with near square pixels. Down-sampling by pixel binning of the X-dimension is applied during ground processing at the same time the resampling occurs to correct the X optical distortions. Therefore, the effective optical distortions along the X dimension are $\frac{1}{4}$ of the pixel size, with the X pixel size being $\sim 75.3\text{m}$ at nadir.

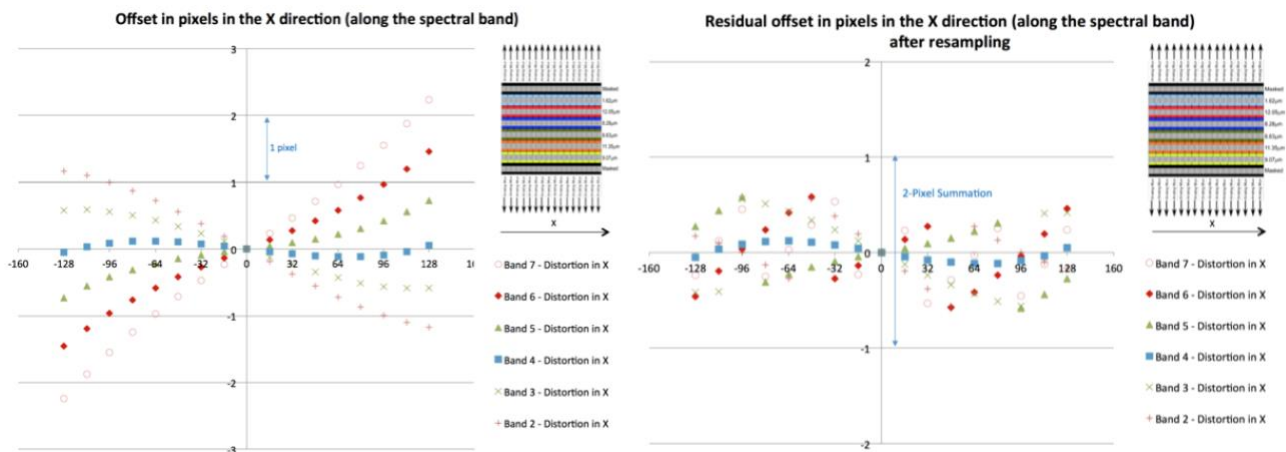


Figure 4: Left: Instrument optical distortions along the X-axis (cross-scan). Right: distortions corrected after nearest neighborhood resampling. After binning by a factor of 2, residuals are $\frac{1}{4}$ of the pixel size. Figure reproduced from [2]

Figure 5 shows the instrument optical distortions along the Y (scan) axis. Distortions can be characterized by a constant offset depending on the spectral band, and once this constant offset is compensated for, all spectral bands exhibit a similar quadratic bias. Because of the 2-pixel smearing along the Y-direction, once the constant offset is compensated for, all spectral bands can be co-registered within a $\frac{1}{4}$ of the effective pixel size. The constant offset is compensated for during on-board processing simply by adding a time-delay to the read output of the sensor.

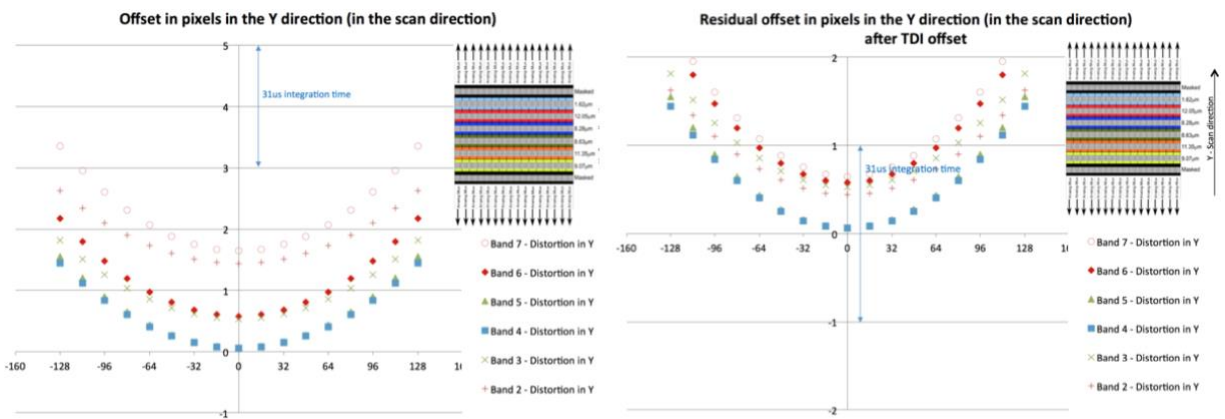


Figure 5: Left: Instrument optical distortions along the Y (scan) direction. Right: On-board time-delay compensates for a constant offset for each spectral bands so that all bands are registered within each other within $\frac{1}{4}$ of the effective resolution. The quadratic bias that is common to all bands is accounted for in the geolocation processing. Figure reproduced from [2]

After performing the constant offset correction along the Y-component and after resampling and binning of the X-component, spectral bands are registered within $\frac{1}{4}$ of the pixel size, and geolocation parameters can therefore be derived for only one master band, with the same geolocation parameters applied to all bands. It is worth noting that the quadratic distortion that remains along the scanning direction is accounted for in the imaging pointing system, and is accounted for in the geolocation computation.

3 ECOSTRESS Pointing Model

Geolocation is derived by propagating the instrument pointing model from the payload on the ISS Japanese Experiment Module Exposed Facility (JEM-EF) site #10 it is mounted on, to the different ISS elements, until it is intersected with the ground topography. These next sections formulate this back-propagation of light from the focal plane back to the ground location it originated from. For this simple model, we will assume a straight propagation of light through the atmosphere.

3.1 Instrument Interior Orientation

After resampling and binning the X-component and compensating for the Y-component constant offset, we derive a pointing model with an equivalent sensor having a single band with 128 pixels in the X dimensions, and where the only distortion left is quadratic along Y (See Figure 6).

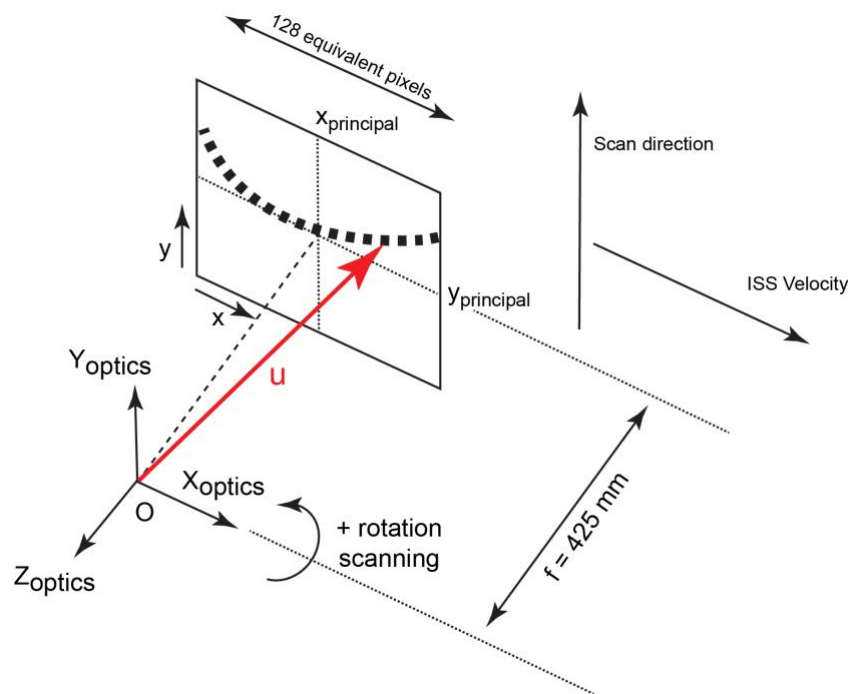


Figure 6: ECOSTRESS equivalent instrument pointing model with 128 pixels in the scan direction and mirror rotation around the X-axis.

For each pixel n , with n between 1 and 128, and given a mirror rotation angle s around the X-axis, we define the instrument pointing model u as follows:

$$\vec{u}(s,n) = \begin{bmatrix} 1 & 0 & 0 & 0 \\ 0 & \cos s & -\sin s & 0 \\ 0 & \sin s & \cos s & 0 \\ 0 & 0 & 0 & 1 \end{bmatrix} \cdot \begin{bmatrix} x(n) - x_p \\ y(n) - y_p \\ -f \\ 0 \end{bmatrix} \quad (1)$$

Where $x(n)$ is the X-coordinate of the equivalent n , $y(n)$ is the Y coordinate of the equivalent pixel n accounting for the quadratic distortion, x_p and y_p are the coordinates of the camera principal point, and f is the instrument focal length.

A note on boresight calibration:

It is common that the instrument and payload axes may not be exactly aligned and that small boresight angles may need to be calibrated during the initial flight calibration. Then defining a 3D rotation matrix $R_{\text{boresight}}$ accounting for boresight angles can be defined so that the calibrated instrument pointing model can be:

$$\vec{u}_{\text{calibrated}}(s,n) = R_{\text{boresight}} \vec{u}(s,n) \quad (2)$$

3.2 From Instrument to Payload Reference Frames

Figure 7 shows the orientation of the Exposed Facility Unit. ECOSTRESS is located on the ISS EFU #10.

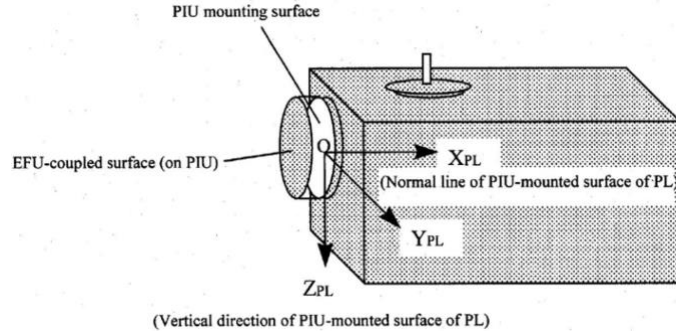


Figure 7: Reference system of Exposed Facility Unit (EFU) as defined in [3]

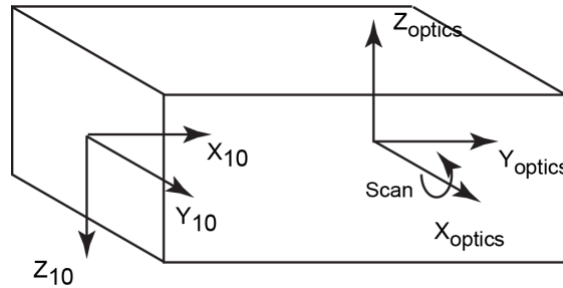


Figure 8: Translation of the reference systems between instrument and EFU.

We can express the change of coordinates from the instrument reference frame to the EFU reference frame as:

$$\begin{pmatrix} X_{10} \\ Y_{10} \\ Z_{10} \\ 1 \end{pmatrix} = \begin{pmatrix} 0 & 1 & 0 \\ 1 & 0 & 0 \\ 0 & 0 & -1 \\ 0 & 0 & 0 \end{pmatrix} \begin{pmatrix} x_{optics}^0 \\ y_{optics}^0 \\ z_{optics}^0 \\ 1 \end{pmatrix} \quad (3)$$

Where the center of the optical instrument in the EFU 10 reference system comes from calibration and is given by:

$$\begin{aligned}
 x_{optics}^0 &= 0.8m \\
 y_{optics}^0 &= -0.022m \\
 z_{optics}^0 &= 0.104m
 \end{aligned}
 \tag{4}$$

3.3 From Payload to Exposed Facility Reference Frames

Figures 9 and 10 present the reference system and the transform between the EFU10 coordinate system and the Japanese Experiment Module Expose Facility ECOSTRESS is mounted on.

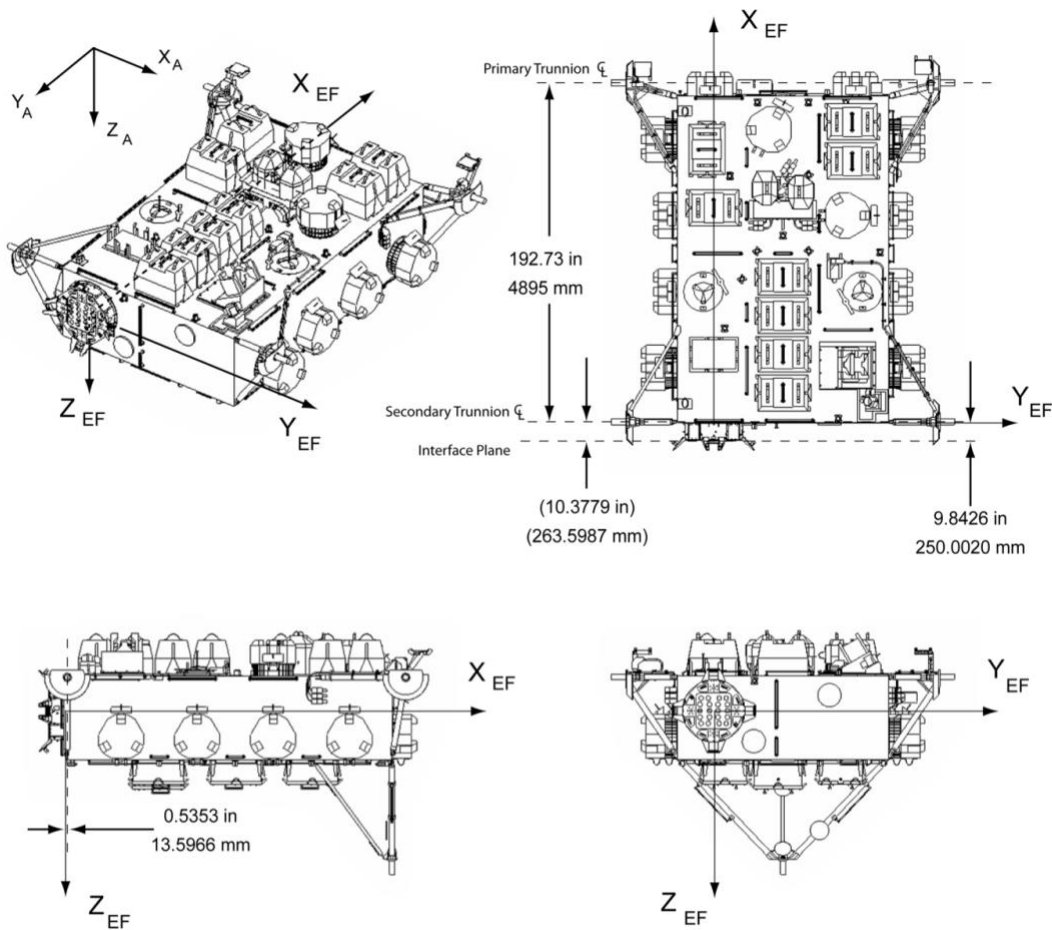


Figure 9: Reference frame of JEM-EF, extracted from [4]

EFU	PL origin [mm] (nominal value)			Installed position [deg.]	Remarks
	X _{EF}	Y _{EF}	Z _{EF}		
#1	794.6	2973.3	382.5	-	+ X ₁ direction = + Y _{EF} direction
#2	794.6	- 973.3	382.5	-	+ X ₂ direction = - Y _{EF} direction
#3	1894.6	2793.1	382.5	-	+ X ₃ direction = + Y _{EF} direction
#4	1894.6	- 793.1	382.5	-	+ X ₄ direction = - Y _{EF} direction
#5	2994.6	2793.1	382.5	-	+ X ₅ direction = + Y _{EF} direction
#6	2994.6	- 793.1	382.5	-	+ X ₆ direction = - Y _{EF} direction
#7	4094.6	2793.1	382.5	-	+ X ₇ direction = + Y _{EF} direction
#8	4094.6	- 793.1	382.5	-	+ X ₈ direction = - Y _{EF} direction
#9	4990.2	2050.0	382.5	-	+ X ₉ direction = + X _{EF} direction
#10	4990.2	- 50.0	382.5	-	+ X ₁₀ direction = + X _{EF} direction
#11	2994.6	1920.0	- 949.8	-	+ X ₁₁ direction = - Z _{EF} direction
#12	4234.6	811.0	- 949.6	28	+ X ₁₂ direction = - Z _{EF} direction

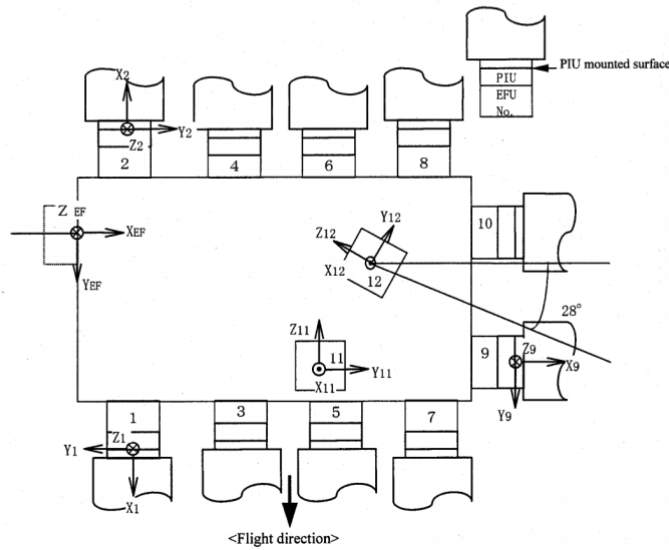


Figure 3.1.3-3 Coordinate System of JEM-EF Payload Mounted Part

Figure 10: EFU10 to JEM-EF reference systems from [3]

This change of reference frames can be expressed as:

$$\begin{pmatrix} \hat{e}_1 \\ \hat{e}_2 \\ \hat{e}_3 \\ \hat{e}_4 \end{pmatrix} X_{EF} \begin{pmatrix} \hat{u}_1 \\ \hat{u}_2 \\ \hat{u}_3 \\ \hat{u}_4 \end{pmatrix} = \begin{pmatrix} \hat{e}_1 \\ \hat{e}_2 \\ \hat{e}_3 \\ \hat{e}_4 \end{pmatrix} \begin{pmatrix} 1 & 0 & 0 \\ 0 & 1 & 0 \\ 0 & 0 & 1 \\ 0 & 0 & 0 \end{pmatrix} \begin{pmatrix} x_{10}^0 \\ y_{10}^0 \\ z_{10}^0 \\ 1 \end{pmatrix} \begin{pmatrix} \hat{u}_1 \\ \hat{u}_2 \\ \hat{u}_3 \\ \hat{u}_4 \end{pmatrix} X_{10} \begin{pmatrix} \hat{u}_1 \\ \hat{u}_2 \\ \hat{u}_3 \\ \hat{u}_4 \end{pmatrix} \begin{pmatrix} 1 \\ 1 \\ 1 \\ 1 \end{pmatrix} \tag{5}$$

with the center of the EFU10 frame within the EF frame given by:

$$\begin{matrix} \uparrow \\ \vdots \\ \uparrow \\ \vdots \\ \uparrow \\ \vdots \\ \uparrow \end{matrix} \begin{matrix} x_{10}^0 = 4.9902m \\ y_{10}^0 = -0.050m \\ z_{10}^0 = 0.3825m \end{matrix} \quad (6)$$

3.4 From Exposed Facility to Japanese Experiment Module Reference Frames

Figure 11 defines the reference system of the Japanese Experiment Module (JEM), and Figure 12 defines the relative reference frames between the JEM and Exposed Facility (EF) module ECOSTRESS is mounted on.

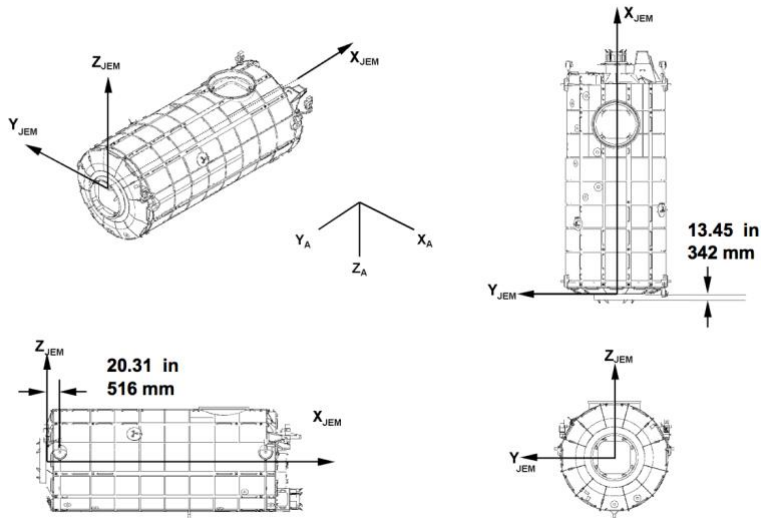


Figure 11: JEM reference frame from [4]

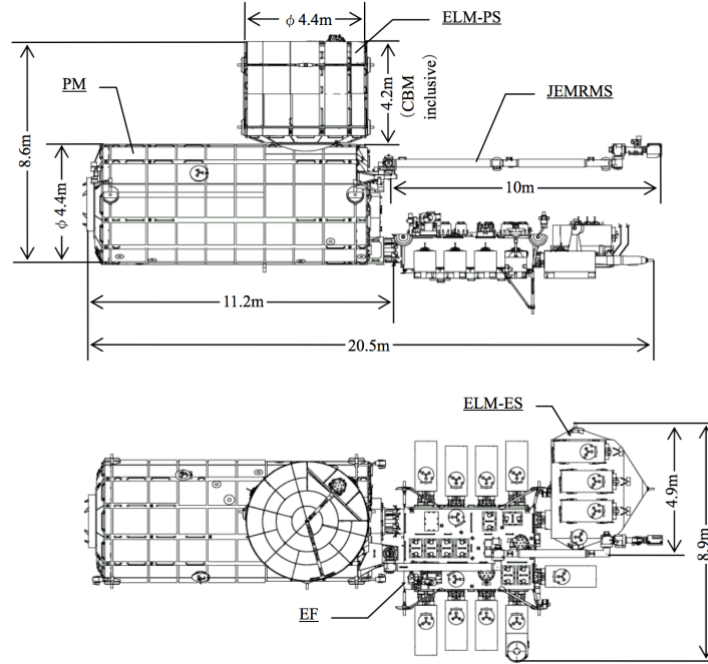


Figure 12: Relative positions of JEM and EF modules from [5]

Change of reference frames between EF and JEM is expressed as:

$$\begin{matrix} \hat{e} \\ \hat{e} \\ \hat{e} \\ \hat{e} \end{matrix} \begin{matrix} X_{JEM} \\ Y_{JEM} \\ Z_{JEM} \\ 1 \end{matrix} \begin{matrix} \hat{u} \\ \hat{u} \\ \hat{u} \\ \hat{u} \end{matrix} \begin{matrix} \hat{e} \\ \hat{e} \\ \hat{e} \\ \hat{e} \end{matrix} \begin{matrix} 1 & 0 & 0 \\ 0 & -1 & 0 \\ 0 & 0 & -1 \\ 0 & 0 & 0 \end{matrix} \begin{matrix} x_{EF}^0 \\ y_{EF}^0 \\ z_{EF}^0 \\ 1 \end{matrix} \begin{matrix} \hat{u} \\ \hat{u} \\ \hat{u} \\ \hat{u} \end{matrix} \begin{matrix} \hat{e} \\ \hat{e} \\ \hat{e} \\ \hat{e} \end{matrix} \begin{matrix} X_{EF} \\ Y_{EF} \\ Z_{EF} \\ 1 \end{matrix} \begin{matrix} \hat{u} \\ \hat{u} \\ \hat{u} \\ \hat{u} \end{matrix} \quad (7)$$

With the center of the EF module in the JEM reference frame given by:

$$\begin{matrix} \uparrow \\ \vdots \\ \uparrow \\ \vdots \\ \uparrow \\ \vdots \\ \uparrow \end{matrix} \begin{matrix} x_{EF}^0 = 11.138m \\ y_{EF}^0 = 0m \\ z_{EF}^0 = -1.685m \end{matrix} \quad (8)$$

It is to note that in [x], z_{EF}^0 is given to be +1.685m. However given the configuration of the modules form Figure 12, we interpret the positive sign as a likely error and use $z_{EF}^0 = -1.685m$.

3.5 From Japanese Experiment Module to ISS Analysis Reference Frames

Figure 13 defines the ISS fixed body axis.

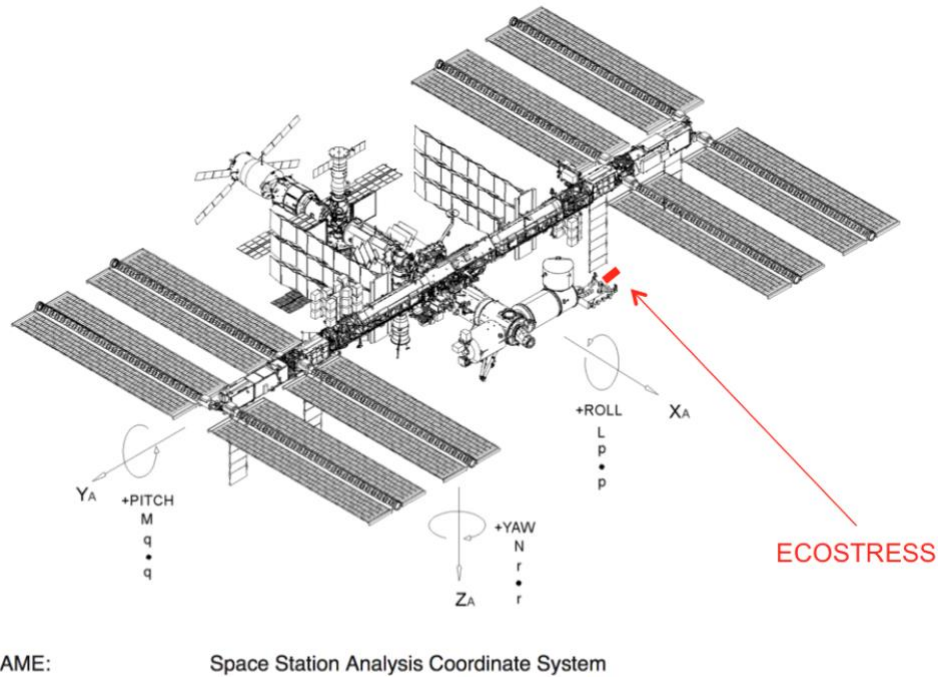


Figure 13: ISS Analysis Coordinate System from [4] and ECOSTRESS location

The change of reference frame between the JEM and the ISS fixed body reference frame is given by:

$$\begin{matrix}
 \hat{e}_A \\
 \hat{e}_A \\
 \hat{e}_A \\
 \hat{e}_A \\
 \hat{e}_A \\
 \hat{e}_A
 \end{matrix}
 \begin{matrix}
 X_A \\
 Y_A \\
 Z_A \\
 1 \\
 \hat{u} \\
 \hat{e}
 \end{matrix}
 \begin{matrix}
 \hat{e} \\
 \hat{e} \\
 \hat{e} \\
 \hat{e} \\
 \hat{e} \\
 \hat{e}
 \end{matrix}
 \begin{matrix}
 0 & -1 & 0 \\
 -1 & 0 & 0 \\
 0 & 0 & -1 \\
 0 & 0 & 0 \\
 1 & 0 & 0 \\
 0 & 0 & 0
 \end{matrix}
 \begin{matrix}
 x_A^0 \\
 y_A^0 \\
 z_A^0 \\
 1 \\
 \hat{u} \\
 \hat{e}
 \end{matrix}
 \begin{matrix}
 \hat{e} \\
 \hat{e} \\
 \hat{e} \\
 \hat{e} \\
 \hat{e} \\
 \hat{e}
 \end{matrix}
 \begin{matrix}
 X_{JEM} \\
 Y_{JEM} \\
 Z_{JEM} \\
 1 \\
 \hat{u} \\
 \hat{e}
 \end{matrix}
 \begin{matrix}
 \hat{u} \\
 \hat{u} \\
 \hat{u} \\
 \hat{u} \\
 \hat{u} \\
 \hat{u}
 \end{matrix}
 \tag{9}$$

According to [3], the center of the JEM reference frame in the ISS fixed body frame is given by:

3.7 From Orbital to Terrestrial Reference Frames

From Figure 14, we define the orbital reference frame (LVLH) axis as:

$$\left\{ \begin{array}{l} \vec{Z}_{LVLH}(t) = -\frac{\vec{P}(t)}{\|\vec{P}(t)\|} \\ \vec{Y}_{LVLH}(t) = \frac{\vec{Z}(t) \times \vec{V}(t)}{\|\vec{Z}(t) \times \vec{V}(t)\|} \\ \vec{X}_{LVLH}(t) = \vec{Y}(t) \times \vec{Z}(t) \end{array} \right. \quad (12)$$

Where $P(t)$ is the ISS position at time t expressed in the Earth centered reference system (CTRS: Conventional Terrestrial Reference System), which for the ISS broadcast data correspond to the WGS-84 reference frame, and $V(t)$ corresponds to the ISS velocity vector at time t , expressed in CTRS. Then, we can express the change of reference frame from the Orbital to the CTRS reference frame with the matrix:

$$M_{Orb2CTRS} = \begin{array}{c} \hat{e} \\ \hat{e} \\ \hat{e} \\ \hat{e} \\ \hat{e} \end{array} \begin{array}{cccc} X_{LVLH}^x & Y_{LVLH}^x & Z_{LVLH}^x & 0 \\ X_{LVLH}^y & Y_{LVLH}^y & Z_{LVLH}^y & 0 \\ X_{LVLH}^z & Y_{LVLH}^z & Z_{LVLH}^z & 0 \\ 0 & 0 & 0 & 1 \end{array} \begin{array}{c} \hat{u} \\ \hat{u} \\ \hat{u} \\ \hat{u} \\ \hat{u} \end{array} \quad (13)$$

3.8 Geolocation on an Ellipsoid

Compiling all the reference frames from the instrument to the Terrestrial reference frames, we write the global transformation matrix as:

$$M_{optics2CTRS}(t) = M_{orb2CTRS}(t)R_p(t)R_r(t)R_y(t)M_{JEM2A}M_{EF2JEM}M_{102EF}M_{optics210}R_{boresight} \quad (14)$$

This transformation matrix only depends on time t as the attitude angles, ISS positions and velocities, are also dependent on time. Then, by propagating the instrument pointing vector u defined in equation (1), we write that a point on the ground of coordinates X at time t was imaged by the pixel n if the following equation is verified:

$$X(t,n) = \vec{P}(t) + M_{optics2CTRS} \cdot [\vec{0}, 1]^T + \lambda \cdot M_{optics2CTRS} \vec{u}(t,n) \quad / > 0 \quad (15)$$

The pointing angle u only depends on time and given pixel n , as the mirror angle is also dependent on time alone. The second term of (15) represents the translation between the ISS center of mass and the optical center and we write it as:

$$\vec{T}_{optics}(t) = M_{optics2CTRS} \cdot [\vec{0}, 1]^T \quad (16)$$

Then, the position of the optical center in terrestrial coordinates is given by:

$$\vec{P}_{optics}(t) = \vec{P}(t) + \vec{T}_{optics}(t) \quad (17)$$

And (15) can be simplified such that:

$$X(t) = \vec{P}_{optics}(t) + \lambda \vec{v}(t,n) \quad \text{for some } / > 0 \quad \text{and} \quad \vec{v} = M_{optics2CTRS} \vec{u} \quad (18)$$

We have the equation of a single ray from the instrument optical center pointing toward the Earth, and to determine the geolocation of pixel n at time t on an Earth ellipsoid with elevation h , we determine $/$ such that X is at the intersection of this ray with the ellipsoid:

$$\frac{X_x^2 + X_y^2}{A^2} + \frac{X_z^2}{B^2} = 1 \quad (19)$$

Using the WGS-84 ellipsoid, we have:

$$\begin{cases} \hat{A} = a + h \\ \hat{B} = b + h \end{cases} \quad \text{with} \quad \begin{cases} \hat{a} = 6378137m \\ \hat{b} = 6356752.3142m \end{cases} \quad (20)$$

This equation can be expanded as a second order polynomial such that

$$\frac{\hat{e}v_x^2 + v_y^2}{\hat{e}A^2} + \frac{v_z^2 \hat{u}}{B^2 \hat{u}} / ^2 + 2 \cdot \frac{\hat{e}P_{optics_x} \cdot v_x + P_{optics_y} \cdot v_y}{\hat{e}A^2} + \frac{P_{optics_z} \cdot v_z \hat{u}}{B^2 \hat{u}} / + \frac{\hat{e}P_{optics_x}^2 + P_{optics_y}^2}{\hat{e}A^2} + \frac{P_{optics_z}^2 \hat{u}}{B^2 \hat{u}} - 1 = 0 \quad (21)$$

Two solutions are obtained, with the smallest one being the one we are looking for (the one one intersecting with the other side of the Earth ellipsoid).

3.9 Geolocation on a Topography Surface

In practice, we are interested in geolocating each pixel on a topography surface to account for topography parallax effects. Intersection of a given ray with a topography model can be achieved iterating the method of equation (21) with a topography surface, as depicted in Figure 15. We find the geolocation of the pixel n with an ellipsoid at a given elevation h_0 . Actual elevation h_1 from the digital elevation model (DEM) is read at the given geolocation, and the ray is projected on the ellipsoid at the new elevation h_1 . This scheme is then iterated until convergence of either the geolocation.

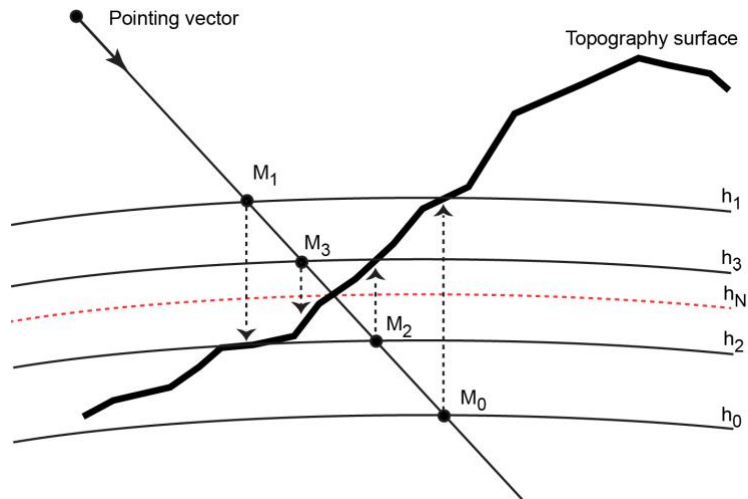


Figure 15: Iterative scheme to derive geolocation using a DEM and ray intersection with ellipsoid at successive heights.

4 ISS Stability Analysis

The previous section detailed how the geolocation of a given pixel can be determined given the instrument characteristics, the ISS positions, velocities, and attitude angles, and geolocation accuracy therefore directly depends on the accuracy of these parameters. In the following paragraphs we explore the impact of the ISS position and attitude angles uncertainties on the geolocation uncertainties.

ISS attitude uncertainties are studied by compiling data from three JAXA accelerometers sampled at 100Hz on-board the JEM-EF platform, and from the HICO star-tracker on-board the JEM, sampled at 1Hz [3]. These attitudes should therefore be very similar to what ECOSTRESS experiences given the location on-board ISS are very close. Figure 16 shows the power spectral density (PSD) of the attitude data recorded for each roll, pitch, and yaw axis.

In the following, geolocation uncertainties are derived from a Monte Carlo simulation where probability density functions on the input parameters are transferred to a probability density function on the geolocation. This model is derived using a flat topography model at zero elevation and the ISS orbit is modeled as a 400km elevation circular orbit with 51.65 degrees.

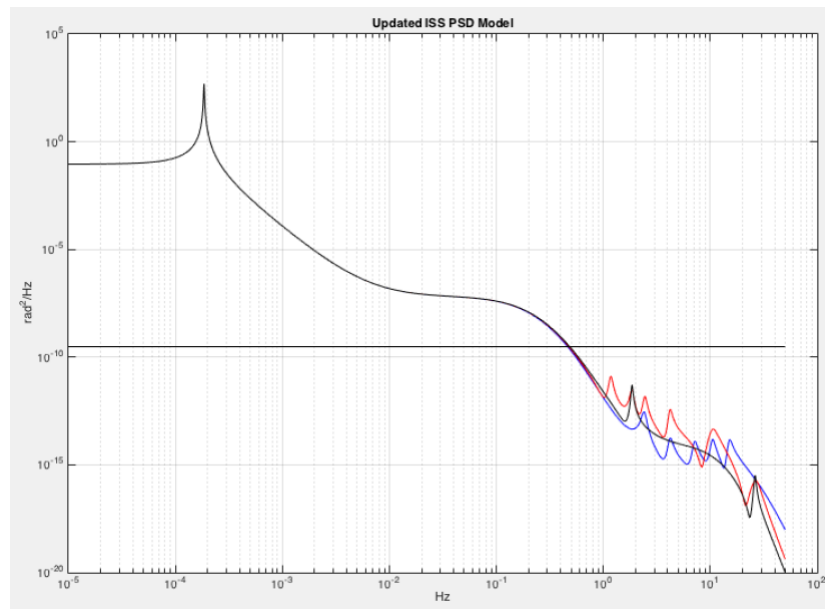


Figure 16: Power Spectral Density (PSD) recorded on the JEM-EF platform for all 3 axis (3 colors). The black line represents the 0.001 deg/axis expected attitude knowledge of the ISS. Reproduced from [3]

4.1 Expected Jitter at 1-Pixel Time-Scale

At the scale of 1-pixel, or 31.6 us, the attitude jitter from the ISS is negligible. The largest error comes from the encoder uncertainty in the rotating mirror, with uncertainty at 1-sigma of $6.9 \cdot 10^{-6}$ rad [1]. This mirror uncertainty produces the maximum geolocation uncertainty for mirror angles of 25 degrees, with geolocation uncertainty of 2.2 m.

4.2 Expected Jitter at 1-Scanline Time-Scale

It takes 1.18s for the ECOSTRESS mirror to complete a half rotation, and that is therefore the time it takes to repeat a scan line (double sided mirror [1]). Corresponding to a frequency of 0.85Hz and integrating the PSD for frequencies above 0.85Hz, we determine an RMS uncertainty of 10^{-4} deg/axis. Taking into account both this uncertainty and the mirror uncertainty translates to a maximum geolocation uncertainty of 2.3m at 1-sigma.

4.3 Expected Jitter at 1-Image Time-Scale

An ECOSTRESS scene is composed of 44 scan-lines and takes 52s to be acquired, corresponding to frequency modes higher than 0.019Hz. Integrating the PSD, we find an RMS uncertainty of 0.005 deg/axis. Taking into account this uncertainty and the mirror uncertainty translates to a maximum geolocation uncertainty of 38m at 1-sigma.

However, we see that the 0.005 deg/axis is greater than the expected 0.001 deg/axis attitude rate knowledge of the ISS [6]. Therefore, the 38 m uncertainty within 1 scene is certainly an upper bound, and if we instead use an uncertainty of the expected 0.001 deg/axis, the geolocation error reduces to 8m at 1-sigma.

4.4 Expected Jitter from Repeat Orbits

Integrating over all frequencies of the PSD produces an RMS uncertainty of 2.52 deg/axis, which would translate to a geolocation error of about 20 km at 1-sigma. From Figure 16, we see that the maximum error happens in the low frequencies, and in particular around the orbital rate. However, at any given time, the ISS on-board instrument are expected to deliver attitude data with 3-sigma uncertainty better than 1 deg/axis for any instrument attached to the ISS [6].

Considering 1/3 deg/axis maximum uncertainty at any given time, the geolocation error becomes 2.5 km at 1-sigma.

4.5 Uncertainty from ISS Position Uncertainty

The ISS position uncertainty is given at 45.8m at 1-sigma, which translates to a maximum geolocation error of 60m at 1-sigma.

4.6 Error Budget of Geolocation

Previous paragraphs have shown that geolocation uncertainties during the acquisition of a given scene are negligible and likely account for a fraction of the image pixel size. We conclude that the relative geolocation accuracy of ECOSTRESS imagery is expected to be meet all requirements.

However, it was also shown that absolute orientation accuracy could suffer due to inaccurate absolute knowledge of the ISS attitude angles. This uncertainty will introduce an absolute geolocation uncertainty of 2.5km at 1-sigma. The next section explains how this absolute error can be minimized.

5 Geolocation Correction Based on Image Matching

Analysis of the geolocation uncertainties in the previous section concluded that the min source of error could be attributed to lack of knowledge of absolute attitude angles. However, relative attitude information is supposed to be known with sufficient accuracy that the corresponding geolocation error should account for less than a fraction of the ECOSTRESS pixel size – the

upper bound at 1-sigma was determined at 38m with most likely value at 8m. Therefore, at the time-scale of a given scene, accurate absolute geolocation can be achieved by solving for a constant offset correction on the ISS attitude data. In practice, we usually solve for an affine or a quadratic correction rather than just an offset to account for potential other unknown errors, if the number of ground control points allows such correction to be reliable.

5.1 Geolocation Correction Principle

The general principle to correct for the absolute geolocation error is to gather ground control points (GCPs) within each scene in order to solve for the missing absolute attitude information. GCPs information are propagated back to the ray-tracing model of section 1, and a correction model is updated such that error with the GCPs is minimized.

In practice, GCPs are gathered automatically using image matching between an ortho-rectified reference and the given ortho-rectified ECOSTRESS frame with improper absolute geolocation.

The general scheme borrows from [8], and is illustrated in Figure 17:

1. Produce an ortho-rectified ECOSTRESS image matching the resolution of the reference imagery,
2. Apply image matching between the ECOSTRESS ortho-image and a reference ortho-image. Image matching is performed using Fourier phase correlation, as described in [8],
3. Filter out mismatches and produce GCPs
4. Use GCPs to update ECOSTRESS projection model
5. Potentially iterate steps 1-4

6. Deliver corrected geolocation information for all image pixels for the ECOSTRESS scene

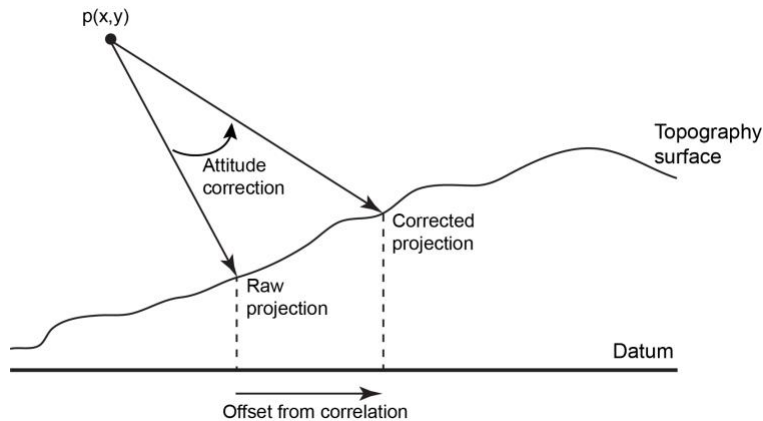


Figure 17: General scheme to update ECOSTRESS absolute attitude uncertainty

The geolocation accuracy after correction should match the level of accuracy given by the image matching. Fourier phase correlation methods have demonstrated matching accuracy to be better than 1/10 of the pixel size [8].

For image matching purpose, ECOSTRESS carries a SWIR band that can easily be matched to the Landsat global reference, offering a high probably of good quality image matching. Given than the Landsat SWIR band absolute geolocation accuracy is given at better than 50 m, ECOSTRESS imagery is expected to achieve a geolocation accuracy on the order of 50m as well.

5.2 Expected Challenges, Failures, and Worst Case Scenarios

Geolocation correction might fail in several instances, when:

- A large part of ECOSTRESS scene is covered by clouds

- A large part of the image is acquired above a water body
- Drastic vegetation changes have occurred between the ECOSTRESS scene and the reference, or when drastic snow cover changes happen

In these instances, image matching cannot be performed and geolocation correction cannot occur. In these low probability cases where geolocation correction might fail, the geolocation error is expected to exhibit an absolute 2.5km uncertainty at 1-sigma. This geolocation error will cause two effects:

1. The immediate effect is the referencing error of the image pixels
2. A secondary effect is a topography distortion in higher-level products because higher level products will be processed with a topography that might be horizontally misplaced by 2.5km at 1-sigma. This effect may not be negligible near the image borders that are acquired at high incidence angles (25 degrees off nadir), in particular in areas of steep slopes.

When the geolocation correction fails, the final user always has the possibility to correct for a simple referencing transformation, but any biases induced by topography artifacts cannot usually be corrected without proper update of the pointing parameters.

6 References

[1] Goullioud, R., 2015. "ECOSTRESS_Error_Budget_2015-04-08.xlsm," NASA/Jet Propulsion Laboratory internal ECOSTRESS Project Document, California Institute of Technology.

- [2] Goullioud, R., 2015. "DatasetSampling&Size20150409.docx," NASA/Jet Propulsion Laboratory internal ECOSTRESS Project Document, California Institute of Technology.
- [3] JEM Payload accommodation handbook – NASDA-ESPC_2900A
- [4] ISS coordinate systems – SSP 30219J, NASA, May 2008
- [5] KIBO Handbook, JAXA, 2007
- [6] S. Gomez and Y. Mesfin, "International Space Station (ISS) Guidance Navigation and Control System (GNC) Memo for Payloads" – Rev D January 2015
- [7] S. Mohan, NASA/JPL, personal communication, 2015
- [8] S. Leprince, S. Barbot, F. Ayoub and J. P. Avouac, "Automatic and Precise Orthorectification, Coregistration, and Subpixel Correlation of Satellite Images, Application to Ground Deformation Measurements", IEEE Transactions on Geoscience and Remote Sensing, Vol.45, No. 6, June 2007.